

# We are IntechOpen, the world's leading publisher of Open Access books Built by scientists, for scientists

6,900

Open access books available

186,000

International authors and editors

200M

Downloads

Our authors are among the

154

Countries delivered to

TOP 1%

most cited scientists

12.2%

Contributors from top 500 universities



WEB OF SCIENCE™

Selection of our books indexed in the Book Citation Index  
in Web of Science™ Core Collection (BKCI)

Interested in publishing with us?  
Contact [book.department@intechopen.com](mailto:book.department@intechopen.com)

Numbers displayed above are based on latest data collected.  
For more information visit [www.intechopen.com](http://www.intechopen.com)



# Anticancer Photodynamic Therapy Using Ruthenium(II) and Os(II)-Based Complexes as Photosensitizers

*Pavel Kaspler, Arkady Mandel, Roger Dumoulin-White and Mark Roufaiel*

## Abstract

Photodynamic therapy (PDT) is an approved procedure using a photosensitizer (PS) activated by light to selectively destroy malignant/premalignant cells. Transition metal complexes, such as Ru(II)- and Os(II)-based PSs (Theralase Technologies Inc., Ontario, Canada), are activated in a wide range of wavelengths, are resistant to photobleaching and have a high singlet oxygen quantum yield and ability to produce cytotoxic reactive oxygen species (ROS). Their design allows fine-tuning of the photophysical and photochemical properties. They demonstrate Type I and II photoreactions, and some are activated in hypoxia. High PDT potency and activation under NIR light and even X-ray may provide an advantage over the approved PSs. Their ability to associate with transferrin (Tf) as an endogenous delivery system increases photobleaching resistance, ROS production, selective cellular uptake, and PDT efficacy in combination with a decreased systemic toxicity. This makes these PSs attractive for systemic therapy of recurrent/progressive cancers. Their PDT efficacy has been demonstrated in various in vitro and in vivo clinically relevant models. The unique properties of the mentioned PSs allow bypassing such limitations of PDT as low specific uptake ratio, insufficiently broad absorption band, and low efficacy in hypoxia. One of these PSs (TLD-1433) was successful against non-muscle invasive urinary bladder cancer unresponsive to contemporary anticancer therapies.

**Keywords:** photodynamic therapy, photosensitizer, transition metal, Ru(II), Os(II), complex, transferrin, selectivity, tumor, cancer, urinary bladder

## 1. Introduction

Photodynamic therapy (PDT) is an actively developing anticancer modality that offers advantages compared to conventional treatments (ionizing radiation and chemotherapy). PDT utilizes two components, light and a photosensitizing compound (PS) activated by light upon photon absorption and producing in its activated state highly cytotoxic reactive oxygen species (ROS) [1]. The attractiveness of PDT is in the use of safe nonthermal doses of light and nontoxic concentrations of the PS and evoking cytotoxic and immunologic effects upon activation of the PS by

light. PDT is supposed to selectively destroy unwanted and/or malignant cells while largely sparing the surrounding healthy tissue. Another desirable property is the ability to induce antigen-specific therapeutic and/or protective immune responses.

Preferential PS uptake by the tumors would make them exclusive targets for cytotoxicity while sparing normal tissues. Light delivery (both source location and emitted energy) can also be controlled more carefully (within the confines of the effective light attenuation in the tissue), which could make PDT a very efficient and safe modality. PDT effects rely upon a variety of photoreactions. The most commonly considered are the two types dependent on oxygen and associated with ROS production: electron transfer from the excited PS generating hydroxyl radical OH among other species (Type I) and energy transfer to a ground-state molecular oxygen  $3O_2$  generating singlet oxygen  $1O_2$  and superoxide radical anions (Type II) [2]. It is proposed that two more types are possible and are oxygen-independent: Type III as the interaction of the activated PS with native free radicals and Type IV as light-induced structural changes in PS allowing it to bind to subcellular targets [3].

PDT has been approved almost 20 years ago as an anticancer treatment. Nevertheless, despite the potential advantages, it is still underutilized clinically. Only a small number of porphyrin- and chlorine-like photosensitizers, as well as one bacteriochlorophyll-based PS, are approved. The number of indications for each photosensitizer is also very limited and includes primarily superficial cancerous/pre-cancerous lesions and other conditions such as actinic keratosis, basal cell carcinoma, high-grade dysplasia in Barrett's esophagus, and age-related macular degeneration. As a palliative measure, PDT is approved for obstructive esophageal or lung cancer and centrally located lung cancer [4, 5]. There are several reasons for this.

One of them is a small depth of penetration of visible light into the tissues restricting PDT to superficial lesions with a thickness not exceeding few millimeters. For deeper organs/tissues, an invasive direct delivery of light is required. Light absorbance of longer wavelengths by the PSs is therefore very advantageous. Light in the range of 650–1350 nm (known as “near-infrared window”) [6] has the greatest penetrating ability into biological tissues. This includes parts of red (625–740 nm) and near-infrared (>750 nm) range that can be used for the PS activation.

Another problem is an unsatisfactory selectivity for malignant tissues resulting in PDT-associated damage of normal tissues. For example, Photofrin® is known for this [4]. Prolonged retention of many porphyrin-based PSs in healthy tissues leads to a problem of sensitivity to sunlight and potentially serious damage to the patients' skin and eye [7, 8]. This could be mitigated by delivery systems selectively targeting malignant cells. These systems employ two modes of action [9]. Passive targeting relies upon the morphological and physiological peculiarities of tumor tissue in combination with physicochemical properties of the PS carrier. Active targeting, in contrast, is based on a molecular recognition of the PS carrier by cancer cells such as binding of specific ligands or antibodies to overexpressed cancer cell receptors. Passive PS delivery systems include nanoparticles, fullerenes, and liposomes and have the advantage of protecting the PS from degradation upon injection. Active systems, on the other hand, have the advantage of improved uptake of the PS. The carriers belonging by themselves to passive targeting systems can be nevertheless supplemented with molecular recognition capacity belonging to the features of active systems, such as decoration with Tf to target Tf receptors overexpressed in malignant cells [10–12]. Nevertheless, smaller active targeting systems (such as PS-Tf conjugates discussed further in this chapter) could have an advantage of greater mobility upon intracellular uptake and potentially the advantage of the blood-brain barrier crossing.

Lastly, PDT-induced ROS production strongly relies upon oxygen availability, which is well known for the porphyrin-based PSs [13, 14]. Deep bulky tumors have

extensive hypoxic regions, which are also associated with the tumor aggressiveness [15, 16]. Although hypoxic regions still can be treated (at a slower rate) by application of fractionated exposure or inducing reperfusion [17, 18], hypoxia severely decreases PDT efficacy [19]. Together with the limited light penetration, this is another reason why PDT in its current state is usually limited to relatively superficial lesions. This problem could be bypassed by PSs employing photoreactions that have little or no dependency on oxygen.

Considering the said above, an advanced PS should have the ability for targeted delivery; penetration through the blood-brain barrier (BBB) and blood-tumor cell barrier (BTCB); activation by a wide range of wavelengths, including NIR light; and employing of different types of photoreactions enabling induction of immune responses to tumor antigens. Solubility in water and/or saline is a great asset for a successful PS as it makes its delivery both easier and safer, without the use of excipients with potential toxicity/side effects on their own.

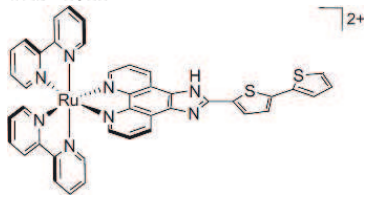
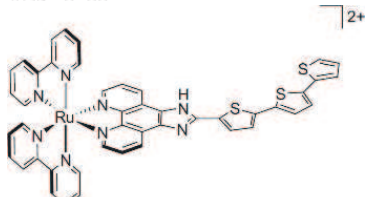
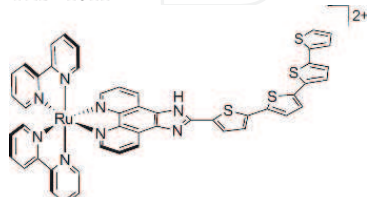
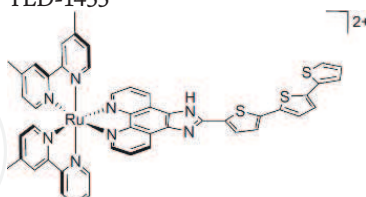
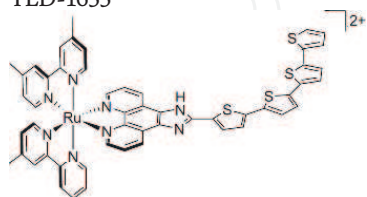
Metal-based coordination complexes are among the obvious candidates to satisfy these requirements. Specifically, transition metal complexes possess a wide range of metal oxidation states and the complex geometries [5, 20]. These complexes (e.g., Ru(II) polypyridyl complexes) are of increasing interest as PSs in photodynamic therapy (PDT) and, more recently, for photochemotherapy (PCT) [21]. Importantly, they can have their properties fine-tuned by choosing the central metal and organic ligands (such as bipyridine and 2,2'-biquinoline). These PSs can employ a great variety of excited states associated with the central metal, ligands, or metal-ligand interactions. This is manifested in photoreactions that are ROS-dependent (Type I/II) or ROS-independent (electron transfer to substrates other than molecular oxygen), excitation at different wavelengths, solubility, systemic toxicity, and finally PDT efficacy. Historically, Pt(IV)-, Ru(II)-, and Rh(III)-based complexes were most actively studied as PSs followed by Ir(III) and Os(II) complexes; see the review by Monro et al. [5]. The examples of the most recent studies [22–26] include a summary on the use of ruthenium complexes as PSs in PDT [27].

This chapter reviews the results obtained by our group and collaborators. The properties and PDT efficacy of Theralase Technologies Inc. PSs [28] and Ru(II)- and Os(II)-based complexes are discussed in the perspective of their clinical application.

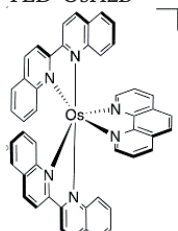
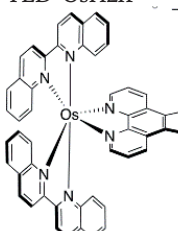
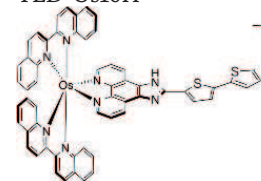
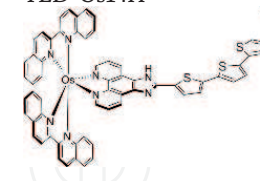
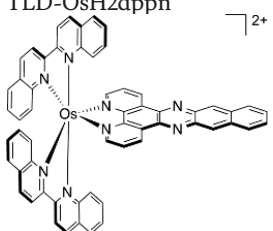
## 2. Physical and chemical properties of the transitional metal-based PSs

### 2.1 Molecular structure

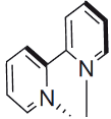
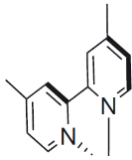
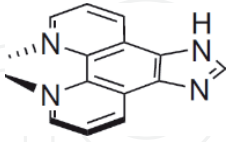
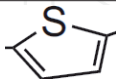
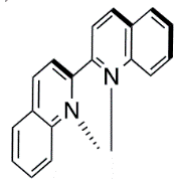
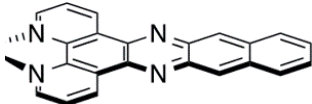
The molecular structure of Ru(II)- and Os(II)-based PSs (later referred to as Ru- and Os-based) is shown in **Tables 1–3**. These are relatively small (approximately 1 kDa) complexes with the ligands involving bipyridine (bip), 2,2'-biquinoline (biq), imidazo[4,5-f][1,10]phenanthroline, and a variable number of thiophene units. A variety of the ligands defines some of the PS properties. For example, the biq ligand is responsible for relatively good absorbance in near-infrared (NIR) light, while the number of thiophene units may be associated with the PS solubility in water [5]. Water solubility, as it was mentioned, represents a serious advantage for this group of PSs as many of the established PSs have poor water solubility [29, 30]. Ru-based PSs are characterized by  $^1\text{O}_2$  quantum yield that is much higher (up to 99%) than for the established (FDA-approved) porphyrin-based PSs: PPIX, an active metabolite of ALA (0.56) and Photofrin (0.89).

<p>TLD-1011</p>  <p>MW = 868.8  <math>^1\text{O}_2</math> quantum yield = 0.74            Fluorescent quantum yield = 0.001</p>	<p>TLD-1411</p>  <p>MW = 950.9  <math>^1\text{O}_2</math> quantum yield <math>\approx</math> 0.99            Fluorescent quantum yield &lt; 0.01</p>	<p>TLD-1611</p>  <p>MW = 1033.1  <math>^1\text{O}_2</math> quantum yield n/d            Fluorescent quantum yield n/d</p>
	<p>TLD-1433</p>  <p>MW = 1007.1  <math>^1\text{O}_2</math> quantum yield <math>\approx</math> 0.99            Fluorescent quantum yield &lt; 0.01</p>	<p>TLD-1633</p>  <p>MW = 1089.2  <math>^1\text{O}_2</math> quantum yield n/d            Fluorescent quantum yield n/d</p>

**Table 1.**  
*Ru(II)-based complexes. Quantum yields are measured in solution rather than in cells.*

<p>TLD-OsH2B <span style="float: right;">2+</span></p>  <p>MW = 954.0  <math>^1\text{O}_2</math> quantum yield = 0.035            Fluorescent quantum yield = 0.0011</p>	<p>TLD-OsH2IP <span style="float: right;">2+</span></p>  <p>MW = 994.0  <math>^1\text{O}_2</math> quantum yield = 0.044            Fluorescent quantum yield = 0.0008</p>	<p>TLD-Os10H <span style="float: right;">2+</span></p>  <p>MW = 1158.2  <math>^1\text{O}_2</math> quantum yield = 0.035            Fluorescent quantum yield = 0.0013</p>	<p>TLD-Os14H <span style="float: right;">2+</span></p>  <p>MW = 1240.3  <math>^1\text{O}_2</math> quantum yield = 0.03            Fluorescent quantum yield = 0.0009</p>
<p>TLD-OsH2dppn <span style="float: right;">2+</span></p>  <p>MW = 1106.1  <math>^1\text{O}_2</math> quantum yield n/d            Fluorescent quantum yield n/d</p>			

**Table 2.** Molecular structures of Os(II)-based complexes. Quantum yields are measured in solution rather than in cells.

Bipyridine	
Methylated bipyridine	
Imidazo[4,5-f][1,10]phenanthroline	
Thiophene	
2,2'-biquinoline	
benzo[i]dipyrido[3,2-a:2',3'-c]phenazine	

**Table 3.**  
Ligands involved in the PSs' molecular structure.

## 2.2 Absorbance spectra

The absorbance spectra of the Ru- and Os-based PSs are shown in **Figure 1**. Among the Ru-based PSs, methylation of bidentate ligands (bip) decreases absorbance. An increase in the number of thiophene rings redshifts the main absorbance peak and eventually results in a considerable increase in absorbance at longer wavelengths (see TLD-1633).

Os-based PSs having biq ligands, in contrast to the Ru-based PSs, have similar spectra. They demonstrate rather uniformly located strong main peak at approximately 340 nm attributed to ligand-centered transitions and a characteristic secondary peak at  $\approx 550$  nm attributed to metal-to-ligand charge transfer (MLCT) centered on the non-biq ligands. Importantly, these PSs demonstrate consistent

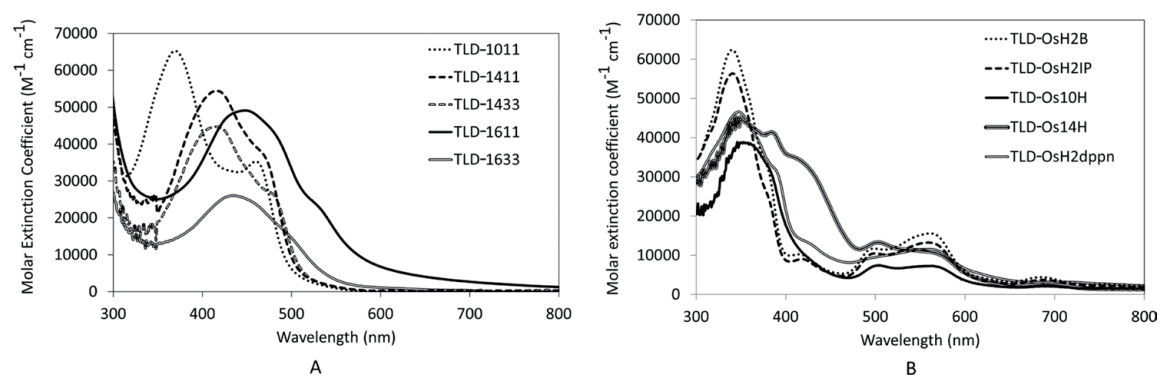


**Figure 1.**  
Absorbance spectra of the Ru(II)- and the Os(II)-based PSs (panels A and B, respectively) in water.

absorbance at longer wavelengths (red to NIR range). The NIR absorbance is attributed to MLCT that involves biq ligands. Altogether, the spectra similarity suggests similar accessible electronic transitions and ground and excited states. Broad absorption band of the Os-based PSs allows for a wider range of photon attenuation coefficients. Considerable absorbance in a clinically important PDT window of 700–900 nm suggests a capacity for one-photon absorption [31]. This asset is emphasized by a good solubility of these PSs in water. Poor solubility in water may hamper PDT potential of PSs even with a good absorbance in this range of the spectrum, as in the case of porphyrin- and phthalocyanine-based PSs [32]. The inclusion of thiophenes and the increase in their number in the ligands (from TLD-OsH2B to TLD-Os14H) not only decreases the main absorbance peak but also markedly redshifts its shape, with a minimal effect on the secondary peak and absorbance in the longer wavelengths (**Figure 1B**).

### 2.3 Photobleaching resistance

If the PS is resistant to photobleaching, this allows less PS being destroyed by the light exposure. In turn, this makes ROS production and subsequent cytotoxic action more efficient, because the process of conversion of photons to cytotoxicity becomes catalytic without stoichiometric consumption of the PS. This allows making the efficacy of PDT treatment independent on the availability of the PS during the treatment.

The bleaching resistance is hence a very valuable property, especially if the delivered light energy must be increased to achieve the desired PDT efficacy. This could be a drawback though in the case of bleaching-based dosimetry during the treatment [33, 34].

Ru-based PSs show notable bleaching under exposure to green light (525 nm). TLD-1433 is slightly more bleaching resistant than TLD-1411 although they have almost identical absorbance at 525 nm. Nevertheless, more than 50% of each PS remains intact even after  $200 \text{ J cm}^{-2}$  of radiant exposure corresponding to  $6.6 \times 10^{19}$  absorbed photons per  $\text{cm}^3$ . Moreover, while bleaching results in the deterioration of the 416–417 nm UV peak, TLD-1433 absorbance in clinically useful range rapidly increases (1.7-fold at 525 nm, 2.0-fold at 625 nm, 1.8-fold at 800 nm) and remains at this level up to the end of light exposure ( $200 \text{ J cm}^{-2}$ ).

Os-based PSs having biq ligands show variable bleaching resistance under green light (525 nm); TLD-OsH2B is the most resistant and TLD-OsH2dppn the most vulnerable. Compared to the Ru-based PS, the bleaching resistance of the Os-based PSs with biq ligands is greater in general, with at least 75% of their initial absorbance retained. The best performers, TLD-OsH2B and TLD-OsH2IP, showed no more than 10% loss of absorbance in the UV peak, with no absorbance loss in green-NIR range. This provides the photobleaching rates in aqueous solution (calculated based on the incident irradiance) equal to  $8.7 \times 10^{-28} \text{ M h} \nu^{-1} \text{ cm}^{-2}$  for TLD-OsH2dppn,  $4.1 \times 10^{-27} \text{ M h} \nu^{-1} \text{ cm}^{-2}$  for TLD-OsH2IP, and  $1.5 \times 10^{-26} \text{ M h} \nu^{-1} \text{ cm}^{-2}$  for TLD-OsH2B [31]. For comparison, the photobleaching rate for the approved PSs can be much higher (by several orders of magnitude):  $5.6 \times 10^{-24} \text{ M h} \nu^{-1} \text{ cm}^{-2}$  for benzoporphyrin derivative mono acid A (BPD),  $7.3 \times 10^{-23} \text{ M h} \nu^{-1} \text{ cm}^{-2}$  for PPIX, and  $4.8 \times 10^{-16} \text{ M h} \nu^{-1} \text{ cm}^{-2}$  for curcumin [35–37].

### 2.4 ROS production

Production of ROS represents a final event of the PS activation by light leading to PDT cytotoxicity. Ru-based TLD-1433 is able to generate hydroxyl radical  $\cdot\text{OH}$  under red light (625 nm,  $119 \text{ mW cm}^{-2}$ ), although singlet oxygen  $^1\text{O}_2$  production is not detected. Importantly, ROS is generated despite very low

absorbance of TLD-1433 in red light. This, however, requires certain molecular and ionic environment because ROS is generated only in incomplete DMEM cell culture medium (not complemented with FBS and antibiotics) but not in DI water despite almost identically low absorbance.

Exposure to NIR light (808 nm, 720 mWcm<sup>-2</sup>) produces some amount of ROS (\*OH), but it at least an order of magnitude less than under red light. This occurs despite a similar number of absorbed photons and absorbance at 808 nm only 18% less than at 625 nm and greater delivered energy. This may suggest that not only the total delivered energy and number of the absorbed photons but also the photon energy is important for the efficacy in ROS production.

### **3. Association of the PSs with transferrin**

#### **3.1 Delivery platforms**

To address the challenge of selective uptake of the PSs by tumors, it would be attractive to utilize serum proteins and natural transmembrane transporters as delivery vehicles. Despite numerous approaches for targeted delivery of the PSs including receptors-assisted uptake (as mentioned in the chapter introduction), neither is related to the use of Tf as a vehicle for transition metal-based complexes. The notable exceptions are the works on the interaction between Tf and Cr(III) complexes [38, 39]. It is also known that Ru(II) complexes can associate with albumin and iron transporter transferrin (Tf) [40, 41]. In addition, overexpression of Tf receptors is a common feature of malignant cells that tend to have an increased Fe<sup>3+</sup> uptake [42]. The effect of the association of Ru(II)-based PSs with Tf on their photophysical and photobiological properties needs however more elucidation.

#### **3.2 Association signatures and effect of Tf on absorbance spectra**

Upon subtraction of the spectra of the complex and Tf from the spectrum of their premix, a characteristic signature of association between the Ru-based complex and Tf can be detected, with two peaks in UV and visible range. The UV peak indicates conformational changes in aromatic rings (the complex itself or transferrin molecule), and the visible range peak is interpreted as an indicator of LMCT (ligand to metal charge transfer) that represents the interaction between the metal of the complex and transferrin [43].

Premixing of Ru-based complexes with apo-Tf (the Tf not saturated with Fe<sup>3+</sup>) at 4:1 molar ratio demonstrates the signature with UV and visible range peaks (**Figure 2A**). The absorbance increase in UV range could be due to conformation changes either in the Tf molecule or the complex (as both have UV maxima at similar wavelengths). The peak in visible range indicates a new spectral component distinct (redshifted) from the comparable absorbance peak for the PS alone. This indicates the complex-Tf association and is related to the interaction between the metal in the complex and the Tf molecule.

There is also an increase in absorbance between the signature peaks and, importantly, in the long wavelength tail of the spectrum in the visible range and further into the NIR, which is clinically relevant for PDT. Notably, the absorbance of TLD-1433 alone is very low in red to NIR. The increase in absorbance upon the association with Tf is 16.2-fold (MEC = 3125 vs. 193 M<sup>-1</sup> cm<sup>-1</sup>) in red (635 nm) and 5.7-fold (MEC = 1676 vs. 294 M<sup>-1</sup> cm<sup>-1</sup>) in NIR (800 nm), compared to 5.0-fold (MEC = 8027 vs. 1600 M<sup>-1</sup> cm<sup>-1</sup>) increase in the green (535 nm). Notably, the ability of the PS to associate with Tf depends on the number of thiophene rings in the complex. One

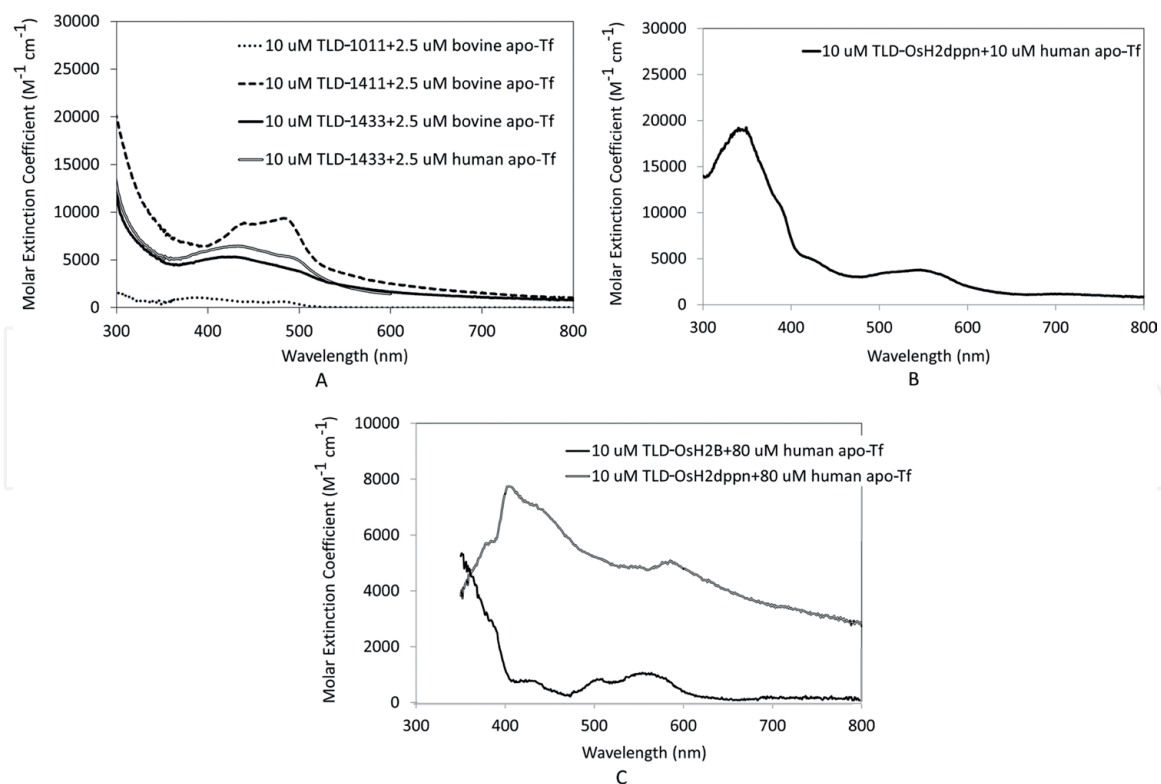


**Figure 2.** Spectral signatures of association of the Ru(II)-based (panel A) and Os(II)-based (panels B and C) PSs with apo-Tf. The incubation of Ru-based PSs was performed in 10 mM phosphate buffer +100 mM NaCl (pH = 7.4) and of Os(II)-based PSs in the phosphate buffer (panel B) or incomplete RPMI1640 cell culture media (panel C).

thiophene ring is not enough for this as evident for TLD-1011. Hence, not only metal but also organic ligands play a role in the association of the complex with Tf.

The association signatures seem to be insensitive to the source of apo-Tf and are very similar for bovine and human Tf. The signatures resemble the signature of Fe<sup>3+</sup>-Tf binding but are not identical to it. Notably, TLD-1433 can also be associated with Fe<sup>3+</sup> saturated holo-Tf although the magnitude of the association signature is lesser than for apo-Tf [43].

Os-based PSs with biq ligands are also able to associate with apo-Tf, but their signatures (**Figure 2C**) are distinct from those of Ru-based PSs. The visible range peak (observed for TLD-OsH2B and TLD-OsH2dppn but not for TLD-OsH2IP) is however more redshifted (in the range of 500–600 nm), and the signature magnitude is much lesser.

### 3.3 Stability of the TLD-1433 + Tf association at low pH

Physiologically, when Tf bound with Fe<sup>3+</sup> is taken up into a cell, it releases iron in endosomes when pH is decreased to ≈5.5 [44]. TLD-1433-Tf conjugate, in contrast, remains stable during the gradual acidification emulating this process [43]. This is evident by the stability of absorbance at the two peaks of the signature across different pH values.

Notably, an association of TLD-1433 with holo-Tf also survives the acid environment. The magnitude of the signature peaks is 31–33% lower than for TLD-1433 & apo-Tf at pH = 7.4, but by pH = 5 it increases so the UV peak magnitude catches up with that of TLD-1433 & apo-Tf, and the visible peak magnitude even becomes about 20% greater. Hence, TLD-1433 may remain associated with Tf in the acidic endosome environment. Acidification resistance does not hold however for the

increased absorbance in green to NIR range. The increase in red-NIR range due to the association of TLD-1433 with Tf deteriorates completely at low pH, and only in the green range, it shows some resistance: 16% remaining for TLD-1433 & apo-Tf and 66% for TLD-1433 & holo-Tf.

### **3.4 Effect of Tf on photobleaching**

Association with Tf markedly decreases the extent and rate of photobleaching of TLD-1433 under green light (525 nm, 130 mWcm<sup>-2</sup>). At 0.93\*10<sup>20</sup> absorbed photons per cm<sup>3</sup>, more than 59% of TLD-1433 remains intact in 1:1 TLD-1433 & Tf premix. At the comparable absorbed light (0.23\*10<sup>20</sup> absorbed photons per cm<sup>3</sup>), 74% of TLD-1433 in the premix persists compared to 45% of TLD-1433 alone [43]. As mentioned above, a decreased bleaching allows for more efficient ROS production with less PS expended, so the advantage of TLD-1433 & Tf conjugate is evident.

### **3.5 Effect of Tf on ROS production**

Association of TLD-1433 with Tf dramatically increases ROS production upon irradiation with red light (625 nm, 119 mWcm<sup>-2</sup>). In this case, <sup>1</sup>O<sub>2</sub> is generated, which does not happen with TLD-1433 alone. The production of \*OH is increased twofold at 1.9\*10<sup>22</sup> absorbed photons per cm<sup>3</sup> [43]. The association with Tf is therefore advantageous for ROS production considering that \*OH is not only an extremely cytotoxic ROS but can also be produced from <sup>1</sup>O<sub>2</sub> [45]. The association with Tf is, however, unable to improve ROS production by TLD-1433 under NIR (808 nm, 720 mWcm<sup>-2</sup>) despite the increase in absorbance in this range.

## **4. In vitro PDT**

Transition metal-based PSs hence are able to absorb light at clinically relevant wavelengths and produce cytotoxic ROS, and the association with Tf is beneficial in that. This warrants assessment of this capacity in biological systems. In vitro, the PDT effects are tested using clinically relevant human cancer cell lines (human glioblastoma U87 cells, human bladder cancer HT1376 cells) or nonhuman cells relevant for preclinical models (rat bladder cancer AY27 cells).

### **4.1 Ru-based PSs**

The comparative efficacy of the Ru-based PSs on U87 cells is shown in **Table 4**. PDT efficacy of the Ru-based PSs can be very efficient in green light (LD50 in sub-nanomolar range) and moderately efficient in red light (LD50 in micromolar range in red light), but they are not active in NIR light. Notably, the efficacy of the PSs in red light is observed despite negligible absorbance (measured in water). In complete cell culture medium (and potentially intracellularly), absorbance in red is increased due to association of the PSs with proteins but is still low compared to that at the shorter wavelengths.

Depending on the PS, the maximal PDT effect did not reach 100% cell kill. The data at 45 Jcm<sup>-2</sup> PDT are not shown, but the increase in the light radiant exposure from 45 to 90 Jcm<sup>-2</sup> significantly (P < 0.05) decreased LD50 for the PDT effect in green light. In red light, the PDT efficacy also could be increased with the increase in the radiant exposure from 45 to 90 and then to 180 Jcm<sup>-2</sup>. This can be explained by the insufficient number of incident photons per a given concentration of the PS at lower radiant exposure but not by a difference in quantum efficacy of the PDT that

U87 cells	Dark	Green	Red	NIR
		530 nm	625 nm	808 nm
		90 Jcm <sup>-2</sup>	90Jcm <sup>-2</sup>	400-600 Jcm <sup>-2</sup>
		108 mWcm <sup>-2</sup>	125 mWcm <sup>-2</sup>	150 mWcm <sup>-2</sup>
TLD-1411	LD50 (μM): 101.5 (CI95 = 87.8–117.4)	LD50 (μM): 0.00595 (CI95 = 0.0050–0.0074)	LD50 (μM): 0.909 (CI95 = n/d-12.36)	Insufficient cell kill
		Maximal kill (%): 49.41 (CI95 = 46.9–52.0)	Maximal kill (%): 71.17 (CI95 = 33.7–124.1)	
	N = 28	N = 9	N = 5	
MEC (water)		2520	151	86
TLD-1433	LD50 (μM): 192.9 (CI95 = 146.8–253.3)	LD50 (μM): 0.00702 (CI95 = 0.00261–0.01891)	LD50 (μM): 3.57 (CI95 = 2.99–4.40)	Inconsistent and low cell kill
		Maximal kill (%): 65.9 (CI95 = 59.1–72.8)	Maximal kill (%): 76.2 (CI95 = 66.7–85.8)	
	N = 118	N = 32	N = 32	
MEC (water)		3094	158	294
TLD-1611	LD50 (μM): 62.9 (CI95 = 44.9–92.5)	LD50 (μM): 0.002 (CI95 = 0.00117–0.0040)	Inconsistent and low cell kill	No cell kill
		Maximal kill (%): 74.8 (CI95 = 65.7–83.9)		
	N = 31	N = 9		
MEC		24,263	4635	1167
TLD-1633	LD50 (μM): 31.13 (CI95 = 14.85 to 63.68)	LD50 (μM): 0.000574 (CI95 = 2.403e-006–0.005691)	Inconsistent and low cell kill	No cell kill
		Maximal kill (%): 100.8 (52.2–171.0)		
	N = 14	N = 6		
MEC (water)		7468	741	0
Photofrin®	LD50 (μM): 2974 (CI95 = 245.5–36,027)	LD50 (μM): 0.20 (CI95 = 0.16–0.25)	LD50 (μM): 0.23 (CI95 = 0.17–0.31)	No cell kill
		Maximal kill (%): 79.7 (CI95 = 72.5–87.0)	Maximal kill (%): 91.8 (CI95 = 83.2–100.4)	
	N = 45	N = 18	N = 26	
MEC (water)		6947	3046	209

The cells were incubated with the PS for 4 h, and the PS was removed before PDT. The dose–response provides LD50 (μM) and maximal cell kill (%) for a green and red light and a cell kill for a fixed PS concentration for NIR light. The data are presented as means and their 95% confidence intervals (SEM for NIR PDT).

**Table 4.**  
*In vitro* PDT efficacy of Ru(II)-based PSs on U87 cells, in comparison to the FDA-approved Photofrin®.

depends only on the photon energy but not on the radiant exposure. The increase in the number of thiophenes in the PS complexes decreases LD50 for the green light and hence increases PDT efficacy. The dark toxicity is however also increasing. In HT1376 cells, LD50 in red light (90 Jcm<sup>-2</sup>) is 15.0 μM (CI95 = 9.1–24.9 μM, N = 30).

This is a greater value than for U87 cells and suggests lesser PDT sensitivity. The total PDT cell kill is however high, 98.5% (CI95 = 85.6–111.4%). Dark toxicity is, in contrast, low, with LD50 exceeding 200  $\mu\text{M}$ . Importantly, the efficacy of the Ru-based PSs exceeds the efficacy of FDA-approved Photofrin® in green light, although not in red light (**Table 4**). Judging by LD50, the Ru-based PSs have higher dark toxicity than Photofrin®, but this is of less importance because, in addition to their solubility in water, they are effective at much lesser, nontoxic concentrations.

Pure PDT effect elucidates the PS efficacy for PDT neglecting its dark toxicity, which is justifiable scientifically to reveal mechanisms of the PS action. Clinically, however, in the case of selective uptake of the PS into cancer cells vs. normal cells, cancer cell kill can be achieved both by PDT-mediated and cytotoxic mechanisms, and the total PDT-induced cell kill becomes relevant. Considering this, total cell kill close to 100% can be achieved in green light in sub-micromolar (20 nM for TLD-1633, 30 nM for TLD-1433, and 200 nM for TLD-1411) or even sub-nanomolar range (0.5 nM for TLD-1611). For comparison, Photofrin® achieved 100% total cell kill in U87 cells only at concentrations above 300 nM.

Clinically, the balance between the efficacy and safety of the PS is characterized by the therapeutic ratio that indicates how far a dose for a desired therapeutic effect is from the dose that causes undesired toxicity. Dividing PDT effect LD50 to dark toxicity LD50 provides small numbers that are not convenient to operate with. It is easier therefore to use inverted therapeutic ratio, ITR = Dark LD50/PDT effect LD50. In U87 cells, ITR = 17,061 for TLD-1411, 27,486 for TLD-1433, 31,460 for TLD-1611, and 54,252 for TLD-1633 under green light PDT. This exceeds the ITR = 14,870 for Photofrin® and shows thus a clear clinical advantage of Ru-based PSs over an established porphyrin-based PS.

## 4.2 Os-based PSs

The comparative efficacy of the Os-based PSs on U87 cells is shown in **Table 5**.

Additionally, in HT1376 cells, TLD-OsH2IP has a dark LD50 > 200  $\mu\text{M}$ , N = 43, red light PDT LD50 = 15.0  $\mu\text{M}$  (CI95 = 9.1–24.9, N = 30), and a NIR light PDT LD50 = 39.0  $\mu\text{M}$  (CI95 = 30.6–49.6, N = 5). TLD-OsH2dppn has dark LD50 = 203.2  $\mu\text{M}$  (CI95 = 190.2–217.1, N = 61), red light PDT LD50 = 4.1  $\mu\text{M}$  (CI95 = 2.9–5.7, N = 26) and NIR light PDT LD50 = 27.4  $\mu\text{M}$  (CI95 = 7.2–100.4, N = 9).

The presence of imidazo[4,5-f][1,10]phenanthroline and adding dppn to the complex increase PDT efficacy of the Os-based PSs, although it does not exceed the efficacy of Ru-based PSs. Similarly to the PDT LD50, ITR of the Os-based PSs in red light is also not better than that of Photofrin®; in U87 cells, ITR = 4.9 for TLD-OsH2B, 24.8 for OsH2IP, and 14.7 for TLD-OsH2dppn. In HT1376 cells, ITR > 13.3 for TLD-OsH2IP and equals to 49.6 for TLD-OsH2dppn. The advantage of the Os-based PSs, however, is their PDT activity in NIR light, which both Ru-based PSs and Photofrin® are lacking. ITR for NIR PDT is greater than 5.1 for TLD-OsH2IP and equal to 7.4 for TLD-OsH2dppn.

Another set of experiments focused at three Os-based PSs with bis ligands [31] supplements the data on red light PDT (625 nm, 90 Jcm<sup>-2</sup>, 450 mWcm<sup>-2</sup>). In U87 cells, TLD-OsH2IP is the most efficient PS (LD50 = 57 ± 4  $\mu\text{M}$ ) exceeding both TLD-OsH2dppn (LD50 = 87 ± 12  $\mu\text{M}$ ) and TLD-OsH2B (125 ± 12  $\mu\text{M}$ ). In HT1376 cells, TLD-OsH2dppn is the most efficient (LD50 = 83 ± 4  $\mu\text{M}$ ); the remaining two PSs have similar LD50 (121 ± 10  $\mu\text{M}$  for TLD-OsH2B and 141 ± 14  $\mu\text{M}$  for TLD-OsH2IP). The inferiority of TLD-OsH2B in red light over the two other PSs is best reproduced across the presented datasets although comparative efficacy of TLD-OsH2IP and TLD-OsH2dppn is less consistent.

U87 cells	Dark	Green	Red	NIR
		530 nm	625 nm	808 nm
		90 Jcm <sup>-2</sup>	90 Jcm <sup>-2</sup>	400-600 Jcm <sup>-2</sup>
		108 mWcm <sup>-2</sup>	125 mWcm <sup>-2</sup>	150 mWcm <sup>-2</sup>
TLD-OsH2B	LD50 (μM):395.7 (CI95 = 323.4–484.1)	LD50 (μM):36.0(CI95 = 19.4–365.4)	LD50 (μM):81.5(CI95 = 16.9–393.3)	Kill (%):32.1 (SEM = 14.3)
		Maximal kill (%): 70.7 (CI95 = 19.9–121.6)	Maximal kill (%): 114.3 (CI95 = 7.6–220.9)	
	N = 43	N = 7	N = 12	N = 4
MEC (water)		12,328	3632	2269
TLD-OsH2IP	LD50 (μM):145.8 (CI95 = 67.6–314.6)	LD50 (μM): 3.1 (CI95 = 2.1–13.2)	LD50 (μM): 12.2 (CI95 = 9.2–15.8)	Kill (%): 63.8 (SEM = 13.5)
		Maximal kill (%): (CI95 = 30.67–107.9)	Maximal kill (%): 54.0 (CI95 = 51.5–56.6)	
	N = 20	N = 10	N = 4	N = 4
MEC (water)		10,761	3119	1957
TLD-OsH2dppn	LD50 (μM): 179.1 (CI95 = 112.6–284.8)	LD50 (μM): 0.16 (CI95 = 0.08–0.34)	LD50 (μM): 12.2 (CI95 = 0.7–577.6)	Inconsistent and low cell kill
		Maximal kill (%): 84.2 (CI95 = 70.5–97.8)	Maximal kill (%): 79.1 (CI95 = -2.0–160.3)	
	N = 20	N = 10	N = 4	
MEC (water)		10,486	4828	2273
TLD-Os14H	LD50 (μM): 141.2 (CI95 = 107.8–185.0)	LD50 (μM): 2.1 (CI95 = 1.6–3.4)	LD50 (μM): 2.4 (CI95 = 1.8–3.3)	Kill (%): 24.2 (SEM = 4.7)
		Maximal kill (%): 59.4 (CI95 = 46.6–72.3)	Maximal kill (%): 78.2 (CI95 = 69.0–87.5)	
	N = 54	N = 33	N = 53	N = 10
MEC (water)		11,716	2914	1376

The cells were incubated with the PS for 4 h, and the PS was removed before PDT. The dose–response provides LD50 (μM) and maximal cell kill (%) for a green and red light and a cell kill for a fixed PS concentration for NIR light. The data are presented as means and their 95% confidence intervals (SEM for NIR PDT).

**Table 5.**  
*In vitro* PDT efficacy of Os(II)-based PSs on U87 cells (90 Jcm<sup>-2</sup>).

Importantly, the dataset presented in [31] provides LD50 for NIR PDT (808 nm, 600 Jcm<sup>-2</sup>, 900 mWcm<sup>-2</sup>), in contrast to the cell kill at a single concentration presented in **Table 5**. TLD-OsH2IP proves to be most effective among the three in U87 cells (LD50 = 45 ± 5 μM), whereas TLD-OsH2B was the most effective PS for HT1376 cells (LD50 = 121 ± 8 μM). For this wavelength, therefore, the efficacy of TLD-OsH2dppn was the lowest, in contrast to the red light PDT.

Concentration-wise, the PDT efficiency is almost always similar in red and NIR light. The exception is greater efficacy of TLD-OsH2dppn in red vs. NIR in HT1376 cells (P < 0.001). In U87 cells, ITR is 3.3–9.6 for red PDT and 4.2–12.0 for NIR

PDT. In HT1376 cells, it is, respectively, 4.6–6.1 and 2.6–6.1. As in the dataset shown in **Table 5**, this is far behind the ITR value for Photofrin®, but considerable PDT activity in NIR is a decisive asset. This advantage is reinforced by the similar LD50 for red and NIR PDT, which means that (at certain light exposure conditions) NIR PDT can be at least not worse than red PDT.

One should remember however that NIR PDT needs much more energy to be delivered, NIR range photons carry less energy, and absorbance is lesser than for the red range. Red light PDT is still more efficient per absorbed photon than NIR PDT because similar LD50 in  $\mu\text{M}$  is achieved at a much lesser number of absorbed photons ( $P < 0.001$ ). Hence, the NIR PDT advantage of the Os-based PSs must be realized by increasing the delivered energy of light. This does not pose a problem because no thermal effects are observed for 808 nm at  $600 \text{ Jcm}^{-2}$ .

### **4.3 Effect of Tf on in vitro PDT efficacy**

Additional apo-Tf increases red light PDT efficacy of the Ru-based TLD-1433 in AY27 cells, together with a decrease in dark toxicity [43]. The PDT improvement effect is however significant (PDT effect LD50 = 11.6–11.9  $\mu\text{M}$  vs. 17.0  $\mu\text{M}$  with no additional Tf,  $P < 0.05$ ) only after a relatively short (30 minutes) TLD-1433 incubation before PDT. If the incubation time is increased to 90 minutes, the beneficial effect of the additional Tf is not anymore evident, masked by the increased TLD-1433 PDT efficacy.

### **4.4 PDT efficacy in hypoxia**

Hypoxia in tumors is one of the major challenges for anticancer therapy because both conventional radiotherapy and PDT rely upon oxygen, a mediator of damage to cancer cells. It is known at the same time that the tumors with hypoxic cores are clinically more aggressive [15].

This means that any modality effective under hypoxic conditions is extremely valuable. Among the four Ru-based and six Os-based PSs, Ru-based TLD-1633 and Os-based TLD-OsH2B proved to be active in hypoxic conditions (at 0.1–0.5%  $\text{O}_2$ ) after red light PDT (625 nm,  $90 \text{ Jcm}^{-2}$ ,  $125 \text{ mWcm}^{-2}$ ). Incubation with ALA (having its metabolite PPIX as photosensitizer) is used as a negative control (an oxygen-dependent PS). For TLD-1633, hypoxia resistance is observed at a concentration as low as 4  $\mu\text{M}$ , with significantly non-zero PDT effect = 67.3% cell kill in normoxia ( $P = 0.022$ ) and 46.2% in hypoxia ( $P = 0.036$ ), at moderate (25% cell kill) dark toxicity. For TLD-OsH2B, PDT effect is evident only at 320  $\mu\text{M}$ . PDT effect reaches significantly non-zero effect: 59.8% in hypoxia ( $P = 0.006$ ) vs. 42.2% in normoxia ( $P = 0.0006$ ), and at considerable (53% kill) dark toxicity. For both PSs, hypoxia resistance occurs at concentrations above the PDT LD50.

It is noteworthy that TLD-1633 is active at low oxygen concentration corresponding to  $\text{pO}_2 = 0.76 \text{ mmHg}$ . It is very encouraging because it is known that anticancer efficacy of conventional treatment progressively decreases at  $\text{pO}_2$  below a critical threshold of 15–35 mmHg [46, 47].

High dark toxicity of the OsH2B hypoxia-effective concentration is a clear limitation, but this demonstrates anyways a possibility of hypoxia-effective Os-based PSs that, as it was shown, have also PDT activity in NIR. NIR light has greater penetration depth into tissues than visible light, and this, together with the PS activity under hypoxia, will pose a double benefit for PDT of bulk tumors.

## 5. In vivo PDT

### 5.1 Selective uptake by tumors

Intracellular accumulation of TLD-1433 was detected earlier, and association with Tf facilitated this process [43]. Hence, one needs to explore whether this translates to the selectivity of TLD-1433 uptake into tumors in vivo.

TLD-1433 is able to accumulate selectively in tumor tissue vs. normal ones even without premixing with Tf. In AY27 rat urinary bladder tumors, characteristic staining can be seen co-localized with tumors (**Figure 3**) 1 h after instillation of 50  $\mu\text{g}/\text{mL}$  TLD-1433.

TLD-1433 accumulation in the tumors is at least one order of magnitude greater than in the adjacent apparently normal tissue:  $77 \pm 18$  mg/kg, N = 6 vs.  $0.4 \pm 0.09$ , N = 6, P = 0.007.

The concentration in a tumor, therefore, reaches estimated 76  $\mu\text{M}$ , which is far exceeding in vitro PDT effect LD<sub>50</sub> for U87 cells in green light (**Table 4**). Moreover, the foci of coloration are visible outside of a major tumor. This suggests a possibility of detection of very small malignant lesions not readily visible macroscopically without staining by the PS.

Association of TLD-1433 with apo-Tf is able to increase selectiveness of the PS accumulation in subcutaneous CT26.WT (murine colon adenocarcinoma) tumors in BalbC mice (**Figure 4**). Four hours after systemic injection of 10 mg/kg TLD-1433 premixed with apo-Tf (molar ratio = 1:1), significantly more TLD-1433 is found in a tumor vs. adjacent muscle tissue (P = 0.038); the selectivity ratio is about 1.8. With TLD-1433 injected, the uptake into a tumor is not significantly different from the adjacent muscle tissue.

Averaging of the individual tumor/muscle uptake ratios for each animal confirms the results shown above. The ratio is significantly above 1 upon injection of the TLD-1433-Tf premix ( $1.81 \pm 0.14$ , N = 5, P = 0.005) indicating the uptake selectivity. With TLD-1433 alone injected, the uptake into the tumors is not selective ( $0.74 \pm 0.18$ , N = 4, P = 0.247). This firmly suggests that the association of TLD-1433 with apo-Tf increases selectivity of TLD-1433 uptake by a tumor. Apo-Tf per se cannot be taken up because it has to bind Fe<sup>3+</sup> to be recognized by the cell surface TfR. Since selective improvement of the uptake of TLD-1433 & apo-Tf premix by the tumors is



**Figure 3.** Accumulation of TLD-1433 in AY27 orthotopic urinary bladder tumors in fisher rats. The bladder was examined 1 h after instillation of 50  $\mu\text{g}/\text{mL}$  TLD-1433. The arrows denote the areas of coloration by TLD-1433 implying its accumulation in the lesions.

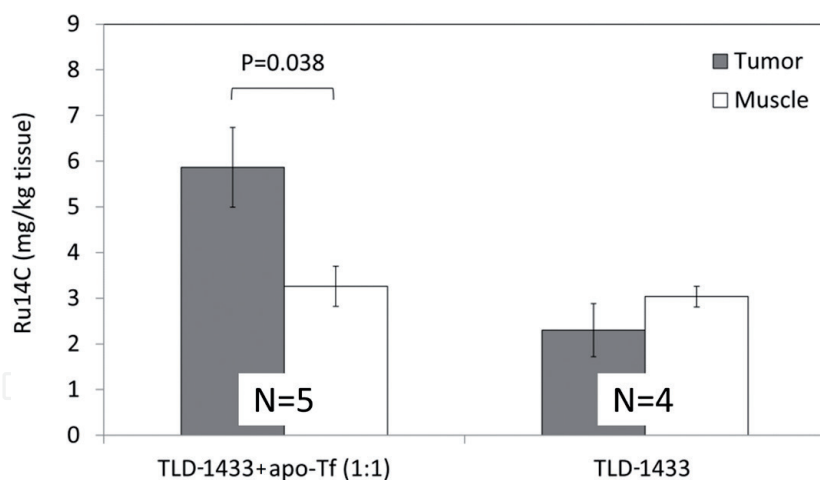


**Figure 4.**

Accumulation of TLD-1433 without or with apo-Tf at different molar ratios in CT26.WT tumors in BalbC mice 4 h after systemic (IV) injection (10 mg/kg). N = 5 for TLD-1433 & apo-Tf group; N = 4 for TLD-1433 group.

demonstrated, one can anticipate two possible scenarios: (1) TLD-1433 & apo-Tf still manages to bind  $Fe^{3+}$ , and (2) TLD-1433 & apo-Tf conjugate can be recognized by TfR and taken up by the cell without the need to bind  $Fe^{3+}$ .

## 5.2 In vivo PDT efficacy

### 5.2.1 Light penetration

Assessing PDT efficacy in vivo is a necessary step on the way to potential clinical applications. It has however its own challenges to be addressed. Light exposure regime is one of them.

The penetration depth of light at different PDT conditions is crucial for the PDT success. For example, a small penetration depth of green light is because of a strong attenuation by intrinsic chromophores, such as hemoglobins and cytochromes. The calculations estimate the energy attenuation up to  $1/8 \text{ cm}^{-1}$  in

TLD-OsH2B	MEC (in water)	No PS	4.5 mg/kg	9 mg/kg	
Green	12,328	0.10–15	0.10	0.01↓	
Red	3632	0.60	0.30↓	0.08↓	
NIR	2269	0.55	0.22↓	0.15↓	
TLD-OsH2IP	MEC (in water)	No PS	2.25 mg/kg	3 mg/kg	9 mg/kg
Green	10,761	0.10–15	0.07↓	0.005↓	0.06↓
Red	3119	0.60	0.70	0.29↓	0.05↓
NIR	1957	0.55	0.79	0.37↓	0.08↓
TLD-Os14H	MEC (in water)	No PS	0.9 mg/kg	1.8 mg/kg	9 mg/kg
Green	11,716	0.10–15	0.04↓	0.06↓	0.06↓
Red	2914	0.60	0.22↓	0.07↓	0.05↓
NIR	1376	0.55	0.11↓	0.08↓	0.08↓

**Table 6.**

Light attenuation in a phantom tumor (proportion of energy penetrating to the bottom of 1-cm-thick phantom vs. surface) in green (525 nm), red (635 nm), and NIR (808 nm) light.

skin and  $1/20 \text{ cm}^{-1}$  in a tumor that has a higher density of vasculature and hence more absorbing chromophores [48]. High absorbance of light by the PS is a very desirable property contributing to its efficacy. This could be a double-edged sword however because high absorbance of the PS close to the tumor surface can shield the deeper tissue from the light exposure and hence result in undertreatment of a tumor. The measurements using a tissue-emulating phantom (a piece of meat having a size of an experimental tumor with an overlaying piece of shaved mouse skin) show indeed that the Os-based PSs (TLD-OsH2B, TLD-Os2IP, and TLD-Os14H) affect the penetration of light into a tumor at different wavelengths. Without PSs, 85–90% of energy is lost across the tumor thickness (about 1 cm) for green (525 nm,  $40 \text{ mWcm}^{-2}$ ), 40% for red (635 nm,  $150 \text{ mWcm}^{-2}$ ) and 45% for NIR (808 nm,  $300 \text{ mWcm}^{-2}$ ) photons. The PSs injected into a tumor further diminishes the light penetration (**Table 6**).

It is noteworthy that the increase in light attenuation across the wavelengths is PS-specific. At the minimal used dose for each PS, TLD-OsH2B does not attenuate green light penetration, TLD-OsH2IP does not attenuate in red and NIR, while TLD-Os14H does this at all three wavelengths. Also, the increase in the PS concentration results in a progressive and disproportional increase in light attenuation. Notably, the absorbance of the PS measured in water (see **Figure 1**) is not translated directly into the PS-dependent light attenuation in the tumor phantom.

The limitations of light penetration can be also illustrated by the distribution of PDT-induced damage in tumors. The damage inflicted by red light (660 nm,  $90 \text{ J/cm}^{-2}$ ,  $125 \text{ mWcm}^{-2}$ ) PDT to CT26.WT subcutaneous tumors in BalbC mice after systemic administration of 10 mg/kg of the 1:1 TLD-1433 & apo-Tf premix clearly diminishes as it goes deeper into a tumor (**Figure 5C,D**). The damage area is not necessarily decreased, but the magnitude of the damage has a definite gradient with coagulative necrosis near the surface and the “general damage” that cannot be defined as coagulative necrosis. The damage is incomplete even when TLD-1433 is associated with apo-Tf (which is expected to facilitate PDT effect as evident from in vitro experiments). Notably, the skin on the way of the light beam is not damaged, which can suggest selectivity of the PS uptake into a tumor. Considering that red light is still delivering 60% of the incident energy at 10 mm depth (**Table 6**), much more shallow damage (up to about 3 mm) suggests a steep gradient of PDT efficacy as the delivered energy falls below a certain threshold.

The observed damage should be clearly attributed to PDT but not dark toxicity of the PS in a tumor because, without light, there is no visible damage (**Figure 5B**).

**Figure 6** shows representative examples of coagulative necrosis as a result of damage and a pattern of gradual transition of the damaged zone from an intact tumor to the necrotic area.

### 5.2.2 Thermal effect

Thermal effect is another consideration because it can potentially occur in a tumor upon light irradiation. For green light, this is possible due to absorption by intrinsic hemoglobin. Hyperthermia is known and used as an anti-tumor modality [49], but in PDT studies, the thermal effect may mask PDT-specific mechanisms of tumor damage.

In the subcutaneous tumor model (CT26.WT tumor in BalbC mice), continuous-wave irradiation with red (635 nm,  $150 \text{ mWcm}^{-2}$ ) or green (525 nm,  $40 \text{ mWcm}^{-2}$ ) light does not show any signs of overheating at the tumor surface. The temperature does not exceed 31–35°C at the end of irradiation even with TLD-Os14H injected intratumorally.

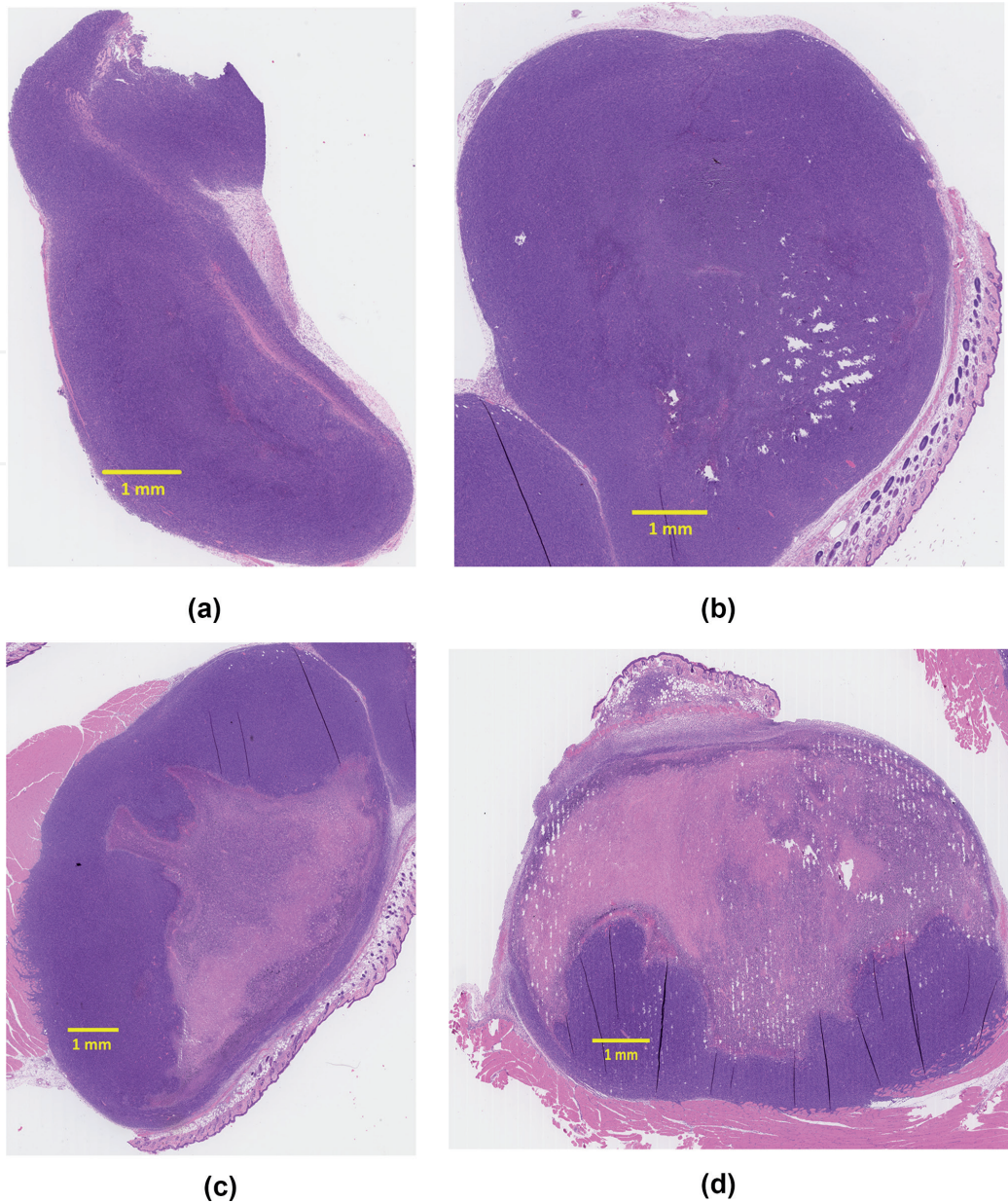


**Figure 5.** Tumor damage (H&E staining) after red light ( $660\text{ nm}$ ,  $90\text{ Jcm}^{-2}$ ,  $125\text{ mWcm}^{-2}$ ) PDT to CT26.WT subcutaneous tumors in BalbC mice after systemic administration of  $10\text{ mg/kg}$  TLD-1433 as 1:1 TLD-1433 & apo-Tf premix. The PDT was performed 4 h after the administration, and the tumors harvested 2 days post-PDT. The Panel a shows untreated tumor, the Panel b shows PS-injected tumor with no irradiation, and the Panels c-d show PDT-treated tumors.

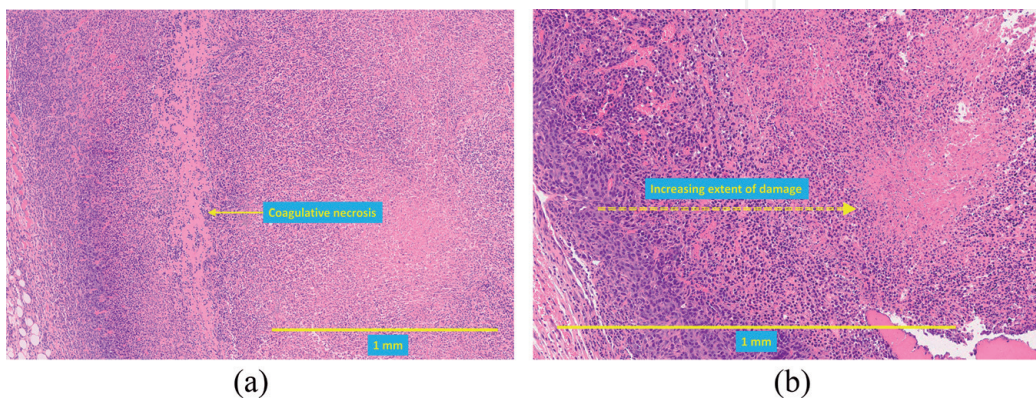


**Figure 6.** Coagulative necrosis and "general damage" in a PDT-treated tumor. The Panel a shows an example of coagulative necrosis area; the Panel b shows a gradient transition from non-damaged tumor area to the necrotic one through the area of "general damage".

Within a tumor, a combination of deeper-penetrating light and less absorbance by the PS also does not result in considerable thermal effect. Under NIR light alone (808 nm,  $600 \text{ Jcm}^{-2}$ ,  $300 \text{ mWcm}^{-2}$ ), the temperature increases only by  $4.8^\circ\text{C}$  (from  $26.9$  to  $31.7^\circ\text{C}$ ) during 30 minutes of irradiation. In the presence of Ru-based TLD-1433 (50 mg/kg intratumorally in  $100 \mu\text{L}$  per 20 g BW), the temperature rapidly increases from  $28.4^\circ\text{C}$  to  $33.6^\circ\text{C}$  (by  $5.2^\circ\text{C}$ ) at  $50 \text{ Jcm}^{-2}$  delivered to a tumor and only by  $8.1^\circ\text{C}$  at the end ( $600 \text{ Jcm}^{-2}$ ). The temperature reaches no more than  $36.5^\circ\text{C}$  showing no PDT-dependent thermal effect. TLD-1433 is responsible only for  $3.3^\circ\text{C}$  (41%) of the total PDT-induced increase. Notably, in euthanized animals, the total increase in temperature is similar to that in live animals (although with more linear increase dynamics). This may mean that the active removal of heat by circulating blood is not critical in maintaining the temperature within the safe range during PDT.

### 5.2.3 PDT effect

In CT26.CL25 subcutaneous tumor model in BalbC mice, intratumoral injection of TLD-1411 or TLD-1433 at 1/20 MTD (1.8 and 5.2 mg/kg, respectively) green ( $525 \text{ nm}$ ,  $192 \text{ Jcm}^{-2}$ ,  $200 \text{ mWcm}^{-2}$ ) light PDT resulted in a fast reduction or complete regression of the tumors and a temporary (8–9 days) delay in their growth [50]. This effect was statistically significant ( $P < 0.05$ ) only for TLD-1433 translating to an increased survival (about 15% of the animals surviving beyond the 90 days follow-up period).

The dose of both PSs has to be increased to 1/2 MTD (18 and 52 mg/kg, respectively) to obtain significant ( $P < 0.01$ – $0.05$ ) PDT effect of greater magnitude, with only continuous-wave PDT effective. About 50% of the animals survived beyond 60 days for TLD-1411 and about 75% beyond 90 days for TLD-1433. **Figure 7** shows an example of the PDT-induced tumor damage and subsequent regression.

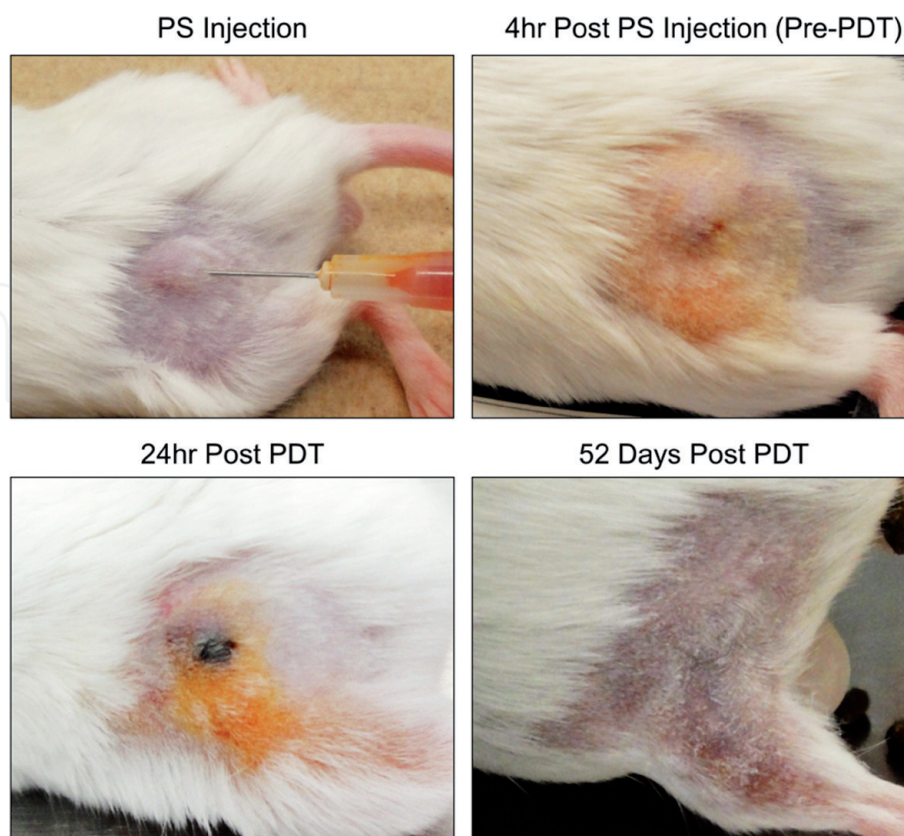


**Figure 7.** An example of successful tumor destruction by 53 mg/kg TD1433-mediated PDT under continuous-wave green light ( $525 \text{ nm}$ ,  $192 \text{ Jcm}^{-2}$ ,  $200 \text{ mWcm}^{-2}$ ).

These results are obtained with a green light that has only a superficial light penetration. TLD-1433-mediated (50 mg/kg = 47% MTD) PDT using deeper-penetrating NIR light (808 nm, 600 Jcm<sup>-2</sup>, 400 mWcm<sup>-2</sup>) does not reach however the efficacy of green light PDT despite 6.7 times greater radiant exposure [43]. Only a trend to improvement in survival (P = 0.164–0.179 vs. dark toxicity and light only) could be observed. This is not surprising by itself considering that TLD-1433 has extremely low absorbance in NIR. Nevertheless, the P values allow hypothesizing that a significant effect could be achieved with more powerful experimental design or greater delivered light energy.

More encouraging is a beneficial effect of combining TLD-1433 with Tf. A highly significant PDT effect in the animals survival can be observed when 4:1 TLD-1433 & apo-Tf premix (50 mg/kg TLD-1433) is injected instead of TLD-1433 only (P = 0.0182–0.0032 vs. dark toxicity and light only). No dark toxicity for tumors (effect of the premix with no light on tumor growth) is detected. Although the difference vs. TLD-1433-induced PDT (P = 0.0633) still does not reach statistical significance threshold, the P value, again, is small enough to talk about a trend toward the improvement. The result reinforces the valuable finding of the benefit of TLD-1433-Tf premix in PDT efficacy improvement under NIR light. This is especially noteworthy because the absorbance of TLD-1433-Tf in NIR range is still very low compared to the absorbance in green light despite the facilitating effect of Tf.

Anyways, 600 Jcm<sup>-2</sup> NIR PDT is able to maintain about 70% of the animals surviving beyond 90 days follow-up (vs. only about 30% after PDT mediated by TLD-1433 that was not mixed with Tf), which is not less than survival after 192 Jcm<sup>-2</sup> green light PDT. This is especially encouraging considering that NIR PDT is not effective *in vitro*, either with or without Tf. The failure to detect *in vitro* PDT effect in NIR is possibly because the short-term viability assay (reflecting metabolic suppression rather than actual cell death) could be not sufficient to detect the effect of NIR that has less energy per photon. The effect *in vivo*, in contrast, is assessed by the long-term follow-up of tumor growth. The activity of the Ru-based complexes under NIR is known from literature [51] but involves multiphoton excitation. In contrast, the results presented above demonstrate the ability of the PSs to be activated by NIR in a continuous-wave regime via single-photon excitation. Moreover, TLD-1433-Tf premix has an additional benefit of decreased systemic toxicity, with MTD more than twofold greater than that for injection of TLD-1433 only [50].

This double benefit of using apo-Tf as a delivery vehicle for TLD-1433 resembles the already mentioned effect *in vitro* for red light PDT using AY27 cells where TLD-1433-Tf decreased dark toxicity and increased PDT efficacy. Note however that *in vitro* experiments using cancer cell line determined dark toxicity in cancer cells and hence can be rather an estimate for dark toxicity of the PS in tumors. In contrast, *in vivo* model considered the benefit for systemic toxicity.

NIR PDT efficacy *in vivo* can be also demonstrated by direct quantitation of the tumor damage. Even suboptimal PDT (200 instead of 600 Jcm<sup>-2</sup>) shows a trend (P = 0.104, df = 8, one-tailed) to an increase in the relative area of damage in a tumor as compared to the tumors not subjected to PDT (dark and tumor alone data pooled). The damage area is increased to 33.4 ± 10.2% (N = 4) vs. 17.1 ± 2.5% (N = 6). The effect is only moderate and does not reach statistical significance, but this could be because of suboptimal (200 Jcm<sup>-2</sup>) radiant exposure.

Among the Os-based PSs (TLD-OsH2B, TLD-OsH2IP, TLD-OsH2dppn), the MTD values vary. TLD-OsH2B is the most toxic (MTD = 1.25 mg/kg) and TLD-OsH2dppn the least toxic (MTD = 47 mg/kg), which is more than one magnitude of difference [31]. For comparison, *in vitro* dark LD50 for three PSs were much closer

to one another (416–617  $\mu\text{M}$  for U87 cells and 476–744  $\mu\text{M}$  for HT1376 cells). As it was mentioned already, however, *in vitro* dark toxicity for cancer cells and *in vivo* MTD as systemic toxicity is not directly comparable.

TLD-OsH2IP-mediated (3 mg/kg = 1/2 MTD) continuous-wave red light PDT (635 nm, 192 or 266  $\text{Jcm}^{-2}$ ) significantly slows down the tumor growth and increases survival vs. light only group ( $P < 0.01$ ). The effect is however temporary (like TLD-1433, as discussed above). Increasing the radiant exposure to 266  $\text{Jcm}^{-2}$  allows for a better result, with the cases of tumor regression and survival significantly increased vs. both dark and light only groups ( $P < 0.01$ ) and about 80% of the animals surviving beyond the 50 days follow-up. Considering high photostability of TLD-OsH2IP, further increase in power and energy density for red light PDT is possible. This could potentially allow achieving complete tumor-suppressing success, at least in the framework of this *in vivo* model.

We have discussed previously that NIR effect is potentially possible even at suboptimal settings with Ru-based TLD-1433-Tf formulation. This formulation has an absorbance in NIR higher than TLD-1433 but still lower than Os-based TLD-OsH2dppn (MEC = 777–1459 vs. 2273  $\text{M}^{-1} \text{cm}^{-1}$ , respectively). Hence, we could expect NIR PDT effect for TLD-OsH2dppn because this PS absorbs much better in NIR than TLD-1433. The PDT effect is indeed observed at 3 mg/kg of the PS and 800 nm and 600  $\text{Jcm}^{-2}$ , with about 60% of the animals surviving beyond 50-day follow-up vs. dark and light only groups ( $P < 0.01$  and 0.0001, respectively). This result further demonstrates the potential of NIR PDT application using transition metal-based PSs. The NIR PDT still requires delivery of at least 3 times more

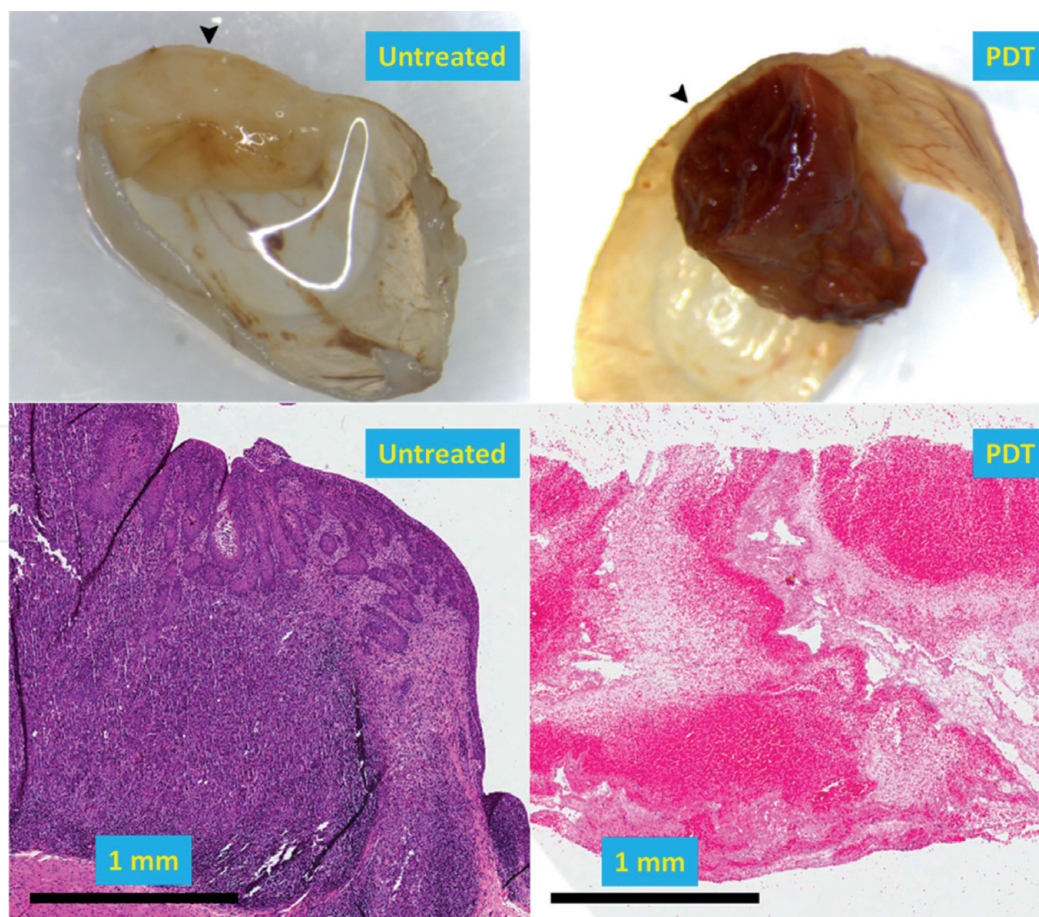


**Figure 8.** Damage to muscle noninvasive AY27 tumor induced orthotopically in fisher rats' urinary bladder 2 days after TLD-1433-mediated green light (535 nm, 90  $\text{Jcm}^{-2}$ ) PDT. TLD-1433 at 6 mg/mL was instilled into bladders, and PDT performed after 1 h of incubation and TLD-1433 washing out of the bladder cavity. The macroscopic image and H&E images are shown.

photons than for red light PDT to match it in efficacy (considering the difference in absorbance and quantum energy), but this does not pose a serious problem because of thermal safety of the light exposure as it was discussed above.

Another anticancer application of PDT using transition metal-based PSs is urothelial non-muscle invasive bladder cancer [52]. As it was mentioned above, Ru-based TLD-1433 accumulated selectively in the orthotopic urinary bladder tumors (instillation with 0.05 mg/mL). At higher concentration of TLD-1433 (6 mg/mL) that is more relevant for the future clinical applications, green light (535 nm, 90 Jcm<sup>-2</sup>) PDT causes full depth (2–3 mm) necrosis in a tumor that showed a deep red coloration (**Figure 8**). Importantly, PDT spared the muscle and urothelial tissue adjacent to the tumors, with only a transient local inflammation of the adjacent urothelium. This is a decisive advantage because the collateral muscle damage impairing the bladder function was a reason for the failure of the prior clinical trials on bladder cancer PDT.

## **6. Clinical PDT efficacy**

The results of the preclinical research allowed planning and initiation of a clinical trial for non-muscle invasive bladder cancer (NMIBC) at the Princess Margaret Cancer Center in Toronto, Canada. It is noteworthy that although several other Ru-based complexes (NAMI-A, KP1019, and KP1339) have currently entered clinical trials as antineoplastic drugs, TLD-1433 is meanwhile the only transition metal complex tested in a trial as a PS for PDT [5, 53].

TLD-1433-mediated PDT (525 nm, 3 W, target dose = 90 Jcm<sup>-2</sup>) with intravesical irradiation demonstrated safety and efficacy of the PS in patients with non-muscle invasive urinary bladder cancer (NMIBC) who were previously unresponsive to contemporary anticancer therapy, including the intravesical therapy with *Bacillus Calmette-Guérin* (BCG) [54]. At therapeutic dose (0.70 mg per cm<sup>2</sup> of bladder surface), 2 of 3 patients were tumor-free at the 180-day posttreatment, with no essential adverse effects and minimal systemic absorption of the PS (complete clearance from the plasma within 72 hrs) and no photosensitivity reactions. This outcome is successful enough to warrant further advance to a phase II trial.

## **7. PS activation by ionizing radiation**

It is worth noting that at least one of the PSs under discussion, TLD-1433, can be activated not only by nonionizing electromagnetic radiation but also by ionizing one (X-ray). Transition metal complexes are theoretically prone to this because the atoms of transitional metals can attenuate X-rays. For example, Ru attenuates X-ray photons at 75 keV to an extent comparable to iodine, an established X-ray imaging agent [55]. Activation of the PS by X-ray is very advantageous because it allows treatment of the tumors located considerably deeper than reachable by NIR. TLD-1433 retains its functionality after 75 keV irradiation at doses up to 20Gy and retains its ability to generate postirradiation \*OH signal under subsequent red light exposure. In cultured human glioblastoma U87 cells, 20 μM TLD-1433 exerted non-zero radio-enhancement effect after 75 keV X-ray exposure (5 Gy) at the magnitude of 37% cell kill (P = 0.020, df = 3), at dark toxicity of 20% cell kill (P = 0.009, df = 3). Moreover, the effect can be detected in vivo in CT26.WT tumors induced in BalbC mice. At 1 Gy, X-ray resulted in a 2.9-fold increase in coagulative necrosis area in the tumors on day 2 postexposure vs. TL1433 alone and X-ray alone groups pooled

( $P = 0.007$ ,  $df = 15$ ) [56]. It is noteworthy that thermal effects at these conditions are highly unlikely because 1 Gy deposits only 0.001 J per gr tissue, which, at the estimated average specific heat capacity  $C \approx 3.7 \text{ J g}^{-1} \text{ K}^{-1}$  [57], provides a very small (0.0003°C) increase in temperature.

## 8. Conclusions

In vitro and in vivo data suggest that transition metal-based complexes are versatile as PSs with diverse photophysical, photochemical, and biological properties. This includes activation over a wide range of wavelengths and high singlet oxygen yield and photobleaching resistance. The Ru(II)-based PSs may have very high cytotoxic efficacy far exceeding the established porphyrin-based PSs. The Os(II)-based PSs are notable in their PDT activity at deeper-penetrating NIR light PDT. Moreover, even Ru(II)-based PSs could be effective in vivo under NIR light. Transition metal-based PSs demonstrate both Type I and Type II photoreactions and can be active in hypoxic conditions, presenting the potential for the treatment of bulky hypoxic tumors. These properties are further facilitated by their ability to associate with endogenous metal transporter molecules, like human apo-Tf, which enables their targeted endocytosis. Furthermore, the association with Tf increases absorptivity at longer wavelengths (far red to NIR range), ROS generation, and finally tumor destroying potential. The observed capacities of the PSs may allow overcoming notorious challenges of PDT: the necessity for deeper light penetration, the selectivity of accumulation in tumors, and activity under hypoxic conditions. Finally, the research has led to the first clinical trial for this class of PSs, with a successful outcome and potential to further clinical advance. This raises justified hopes that with the ongoing technological improvements, such as the development of transition metal complexes (including the advanced Theralase PSs discussed above), and personalized dosimetry with a treatment planning approach, PDT has the potential to become integrated into the mainstream of cancer treatment.

## Acknowledgements

The authors are grateful to the employees of Theralase Inc. for ensuring a very helpful and benevolent working atmosphere and particularly appreciate the contribution of the members of its research team, both past (Jamie Fong, Kamola Kasimova, Yaxal Arenas, and Savo Lazic) and present (Manjunatha Ankathatti Munegowda) for their experimental work and publications used in this chapter. The next acknowledgement is of the invaluable help and crucial support by Prof. Lothar Lilge at Princess Margaret Cancer Centre, Toronto, Ontario, Canada, and his group (including Sarah Forward and Carl Fisher) and of the staff of the other departments, facilities, and services at the center for doing their best to make our work going smoothly and effectively. We greatly appreciate the collaboration with Prof. Sherri McFarland at Acadia University, Wolfville, Nova Scotia, Canada, and her group.

## Conflict of interest

No conflict of interest has been declared.

IntechOpen

IntechOpen

### **Author details**

Pavel Kaspler\*, Arkady Mandel, Roger Dumoulin-White and Mark Roufaiel  
Theralase Inc., Toronto, Canada

\*Address all correspondence to: [pkaspler@theralase.com](mailto:pkaspler@theralase.com)

### **IntechOpen**

---

© 2020 The Author(s). Licensee IntechOpen. This chapter is distributed under the terms of the Creative Commons Attribution License (<http://creativecommons.org/licenses/by/3.0>), which permits unrestricted use, distribution, and reproduction in any medium, provided the original work is properly cited. 

## References

- [1] Henderson BW, Dougherty TJ, editors. *Photodynamic Therapy: Basic Principles and Clinical Applications*. 1st. ed. London: CRC Press; 1992. 480 p
- [2] Dolmans DEJGJ, Fukumura D, Jain RK. Photodynamic therapy for cancer. *Nature Reviews. Cancer*. 2003;**3**:380-387. DOI: 10.1038/nrc1071
- [3] Scherer KM, Bisby RH, Botchway SW, Parker AW. New approaches to photodynamic therapy from Type I, II and III to Type IV using one or more photons. *Anti-Cancer Agents in Medicinal Chemistry*. 2017;**17**:171-189. DOI: 10.2174/1871520616666160513131723
- [4] Van Straten D, Mashayekhi V, de Bruijn H, Oliveira S, Robinson D. Oncologic photodynamic therapy: Basic principles, current clinical status and future directions. *Cancers*. 2017;**9**:1, E19-54. DOI: 10.3390/cancers9020019
- [5] Monro S, Colón KL, Yin H, Roque J 3rd, Konda P, Gujar S, et al. Transition metal complexes and photodynamic therapy from a tumor-centered approach: Challenges, opportunities, and highlights from the development of TLD-1433. *Chemical Reviews*. 2018. DOI: 10.1021/acs.chemrev.8b00211 [Epub ahead of print]
- [6] Smith AW, Mancini MC, Nie S. Bioimaging: Second window for in vivo imaging. *Nature Nanotechnology*. 2009;**4**:710-711. DOI: 10.1038/nnano.2009.326
- [7] Matsuoka M, editor. *Infrared Absorbing Dyes*. New York: Springer Science+Business Media; 1990. 220 p
- [8] Dougherty TJ, Gomer CJ, Henderson BW, Jori G, Kessel D, Korblik M, et al. Photodynamic therapy. *Journal of the National Cancer Institute*. 1998;**90**:889-905
- [9] Hodgkinson N, Kruger CA, Abrahamse H. Targeted photodynamic therapy as potential treatment modality for the eradication of colon cancer and colon cancer stem cells. *Tumour Biology*. 2017;**39**:1-17. DOI: 10.1177/1010428317734691
- [10] Zhang H, Hou L, Jiao X, Ji Y, Zhu X, Zhang Z. Transferrin-mediated fullerenes nanoparticles as Fe<sup>2+</sup>-dependent drug vehicles for synergistic anti-tumor efficacy. *Biomaterials*. 2015;**37**:353-366. DOI: 10.1016/j.biomaterials.2014.10.031
- [11] Gijssens A, Derycke A, Missiaen L, De Vos D, Huwyler J, Eberle A, et al. Targeting of the photocytotoxic compound AIPcS4 to Hela cells by transferrin conjugated PEG-liposomes. *International Journal of Cancer*. 2002;**101**:78-85. DOI: 10.1002/ijc.10548
- [12] Paszko E, Vaz GM, Ehrhardt C, Senge MO. Transferrin conjugation does not increase the efficiency of liposomal Foscan during in vitro photodynamic therapy of oesophageal cancer. *European Journal of Pharmaceutical Sciences*. 2013;**48**:202-210. DOI: 10.1016/j.ejps.2012.10.018
- [13] Bonnett R. *Chemical Aspects of Photodynamic Therapy*. 1st ed. London: CRC Press; 2000. 324 p
- [14] Ethirajan M, Chen Y, Joshi P, Pandey RK. The role of porphyrin chemistry in tumor imaging and photodynamic therapy. *Chemical Society Reviews*. 2011;**40**:340-362. DOI: 10.1039/b915149b
- [15] Pouysségur J, Dayan F, Mazure NM. Hypoxia signalling in cancer and approaches to enforce tumour regression. *Nature*. 2006;**441**:437-443. DOI: 10.1038/nature04871

- [16] Noman MZ, Messai Y, Carré T, Akalay I, Méron M, Janji B, et al. Microenvironmental hypoxia orchestrating the cell stroma cross talk, tumor progression and antitumor response. *Critical Reviews in Immunology*. 2011;**31**:357-377. DOI: 10.1615/CritRevImmunol.v31.i5.10
- [17] Freitas I. Role of hypoxia in photodynamic therapy of tumors. *Tumori*. 1985;**71**:251-259. DOI: 10.1177/030089168507100306
- [18] Dang J, He H, Chen D, Yin L. Manipulating tumor hypoxia toward enhanced photodynamic therapy (PDT). *Biomaterials Science*. 2017;**5**:1500-1511. DOI: 10.1039/c7bm00392g
- [19] Feng L, Cheng L, Dong Z, Tao D, Barnhart TE, Cai W, et al. Theranostic liposomes with hypoxia-activated prodrug to effectively destruct hypoxic tumors post photodynamic therapy. *ACS Nano*. 2017;**11**:927-937. DOI: 10.1021/acsnano.6b07525
- [20] Ashfaq M, Najam T, Shah SS, Ahmad MM, Shaheen S, Tabassum R, et al. DNA binding mode of transition metal complexes, a relationship to tumor cell toxicity. *Current Medicinal Chemistry*. 2014;**2**:3081-3094. DOI: 10.2174/0929867321666140601201803
- [21] Rohrabough TN, Collins KA, Xue C, White JK, Kodanko JJ, Turro C. New Ru(ii) complex for dual photochemotherapy: Release of cathepsin K inhibitor and  $1O_2$  production. *Dalton Transactions*. 2018;**47**:11851-11858. DOI: 10.1039/c8dt00876k
- [22] Ellahioui Y, Patra M, Mari C, Kaabi R, Karges J, Gasser G, Gómez-Ruiz S. Mesoporous silica nanoparticles functionalised with a photoactive ruthenium(ii) complex: Exploring the formulation of a metal-based photodynamic therapy photosensitiser. *Dalton Transactions* 2018. DOI: 10.1039/c8dt02392a [Epub ahead of print]
- [23] Le Gall T, Lemerrier G, Chevreux S, Tücking KS, Ravel J, Thétiot F, et al. Ruthenium (II) polypyridyl complexes as photosensitizers for antibacterial photodynamic therapy: A structure-activity study on clinical bacterial strains. *ChemMedChem*. 2018;**13**: 2229-2239. DOI: 10.1002/cmdec.201800392
- [24] Lin K, Zhao ZZ, Bo HB, Hao XJ, Wang JQ. Applications of ruthenium complex in tumor diagnosis and therapy. *Frontiers in Pharmacology*. 2018;**9**:1323. DOI: 10.3389/fphar.2018.01323. eCollection 2018.
- [25] Pickens RN, Neyhouse BJ, Reed DT, Ashton ST, White JK. Visible light-activated co release and  $^1O_2$  photosensitizer formation with Ru(II),Mn(I) complexes. *Inorganic Chemistry*. 2018;**57**:11616-11625. DOI: 10.1021/acs.inorgchem.8b01759
- [26] Zhang P, Huang H. Future potential of osmium complexes as anticancer drug candidates, photosensitizers and organelle-targeted probes. *Dalton Transactions*. 2018;**47**:14841-14854. DOI: 10.1039/c8dt03432j
- [27] Lilje L. Use of ruthenium complexes as photosensitizers in photodynamic therapy. In: Holder AA, Lilje L, Browne WR, Lawrence MAW, Bullock JL Jr, editors. *Ruthenium Complexes. Photochemical and Biomedical Applications*. Weinheim, Germany: Wiley-VCH Verlag GmbH & Co. KGaA; 2017. pp. 117-137. DOI: 10.1002/9783527695225
- [28] Metal-Based Coordination Complexes as Photodynamic Compounds and Their Use. US Provisional Patent #61801674. Filed Mar 15 2013; US nonprovisional/PCT

application filed Mar. 17, 2014, PCT/  
US14/30194

[29] Li Y, Wang J, Zhang X, Guo W, Li F, Yu M, et al. Highly water-soluble and tumor-targeted photosensitizers for photodynamic therapy. *Organic & Biomolecular Chemistry*. 2015;**13**: 7681-7694. DOI: 10.1039/c5ob01035g

[30] Uruma Y, Nonomura T, Yen PY, Edatani M, Yamamoto R, Onuma K, et al. Design, synthesis, and biological evaluation of a highly water-soluble psoralen-based photosensitizer. *Bioorganic & Medicinal Chemistry*. 2017;**25**:2372-2377. DOI: 10.1016/j.bmc.2017.02.050

[31] Lazic S, Kaspler P, Shi G, Monroe S, Sainuddin T, Forward S, et al. Novel osmium-based coordination complexes as photosensitizers for panchromatic photodynamic therapy. *Photochemistry and Photobiology*. 2017;**93**:1248-1258. DOI: 10.1111/php.12767

[32] Chin Y, Lim SH, Zorlu Y, Ahsen V, Kiew LV, Kiew LV, et al. Improved photodynamic efficacy of Zn(II) phthalocyanines via glycerol substitution. *PLoS One*. 2014;**9**:e97894. DOI: 10.1371/journal.pone.0097894

[33] Wilson BC, Patterson MS, Lilge L. Implicit and explicit dosimetry in photodynamic therapy: A new paradigm. *Lasers in Medical Science*. 1997;**12**:182-199. DOI: 10.1007/BF02765099

[34] Pogue BW, Elliott JT, Kanick SC, Davis SC, Samkoe KS, Maytin EV, et al. Revisiting photodynamic therapy dosimetry: Reductionist & surrogate approaches to facilitate clinical success. *Physics in Medicine and Biology*. 2016;**61**:R57-R89. DOI: 10.1088/0031-9155/61/7/R57

[35] Aveline B, Hasan T, Redmond RW. Photophysical and photosensitizing

properties of benzoporphyrin derivative monoacid ring a (BPD-MA). *Photochemistry and Photobiology*. 1994;**59**:328-335. DOI: 10.1111/j.1751-1097.1994.tb05042.x

[36] Dovigo LN, Pavarina AC, Ribeiro APD, Brunetti IL, Costa CA de S, Jacomassi DP, et al. Investigation of the photodynamic effects of curcumin against *Candida albicans*. *Photochemistry and Photobiology*. 2011;**87**:895-903. DOI: 10.1111/j.1751-1097.2011.00937.x

[37] Valentine RM, Brown CTA, Moseley H, Ibbotson S, Wood KJ. Monte Carlo modeling of in vivo protoporphyrin IX fluorescence and singlet oxygen production during photodynamic therapy for patients presenting with superficial basal cell carcinomas. *Journal of Biomedical Optics*. 2011;**16**:048002. DOI: 10.1117/1.3562540

[38] Toneatto J, Garcia PF, Argüello GA. Advances on the interaction of polypyridyl Cr(III) complexes with transporting proteins and its potential relevance in photodynamic therapy. *Journal of Inorganic Biochemistry*. 2011;**105**:1299-1305. DOI: 10.1016/j.jinorgbio.2011.07.013

[39] Garcia PF, Toneatto J, Silvero MJ, Argüello GA. Binding of [Cr(phen)<sub>3</sub>]<sup>(3+)</sup> to transferrin at extracellular and endosomal pHs: Potential application in photodynamic therapy. *Biochimica et Biophysica Acta*. 2014;**1840**:2695-2701. DOI: 10.1016/j.bbagen.2014.06.010

[40] Dömötör O, Hartinger CG, Bytzeck AK, Kiss T, Keppler BK, Enyedy EA. Characterization of the binding sites of the anticancer ruthenium(III) complexes KP1019 and KP1339 on human serum albumin via competition studies. *Journal of Biological Inorganic*

Chemistry. 2013;**18**:9-17. DOI: 10.1007/s00775-012-0944-6

[41] Śpiewak K, Brindell M. Impact of low- and high-molecular-mass components of human serum on NAMI-A binding to transferrin. *JBIC, Journal of Biological Inorganic Chemistry*. 2015;**20**:695-703. DOI: 10.1007/s00775-015-1255-5

[42] Shen Y, Li X, Dong D, Zhang B, Xue Y, Shang P. Transferrin receptor 1 in cancer: A new sight for cancer therapy. *American Journal of Cancer Research*. 2018;**8**(6):916-931 eCollection 2018

[43] Kaspler P, Lazic S, Forward S, Arenas Y, Mandel A, Lilge L. A ruthenium(II) based photosensitizer and transferrin complexes enhance photo-physical properties, cell uptake, and photodynamic therapy safety and efficacy. *Photochemical & Photobiological Sciences*. 2016. [Epub ahead of print]. DOI: 10.1039/c5pp00450k

[44] Quarles CD Jr, Randunu KM, Brumaghim JL, Marcus RK. Metal retention in human transferrin: Consequences of solvent composition in analytical sample preparation methods. *Metallomics*. 2011;**3**:1027-1034. DOI: 10.1039/c1mt00094b

[45] Ueda J, Takeshita K, Matsumoto S, Yazaki K, Kawaguchi M, Ozawa T. Singlet oxygen-mediated hydroxyl radical production in the presence of phenols: Whether DMPO-<sup>\*</sup>OH formation really indicates production of <sup>\*</sup>OH? *Photochemistry and Photobiology*. 2007;**77**:165-170. DOI: 10.1562/0031-8655(2003)0770165SOMHRP2.0.CO2

[46] Höckel M, Vaupel P. Tumour hypoxia: Definitions and current clinical, biologic, and molecular aspects. *Journal of the National Cancer Institute*. 2001;**93**:266-276. DOI: 10.1093/jnci/93.4.266

[47] Hu YL, DeLay M, Jahangiri A, Molinaro AM, Rose SD, Carbonell WS, et al. Hypoxia-induced autophagy promotes tumour cell survival and adaptation to antiangiogenic treatment in glioblastoma. *Cancer Research*. 2012;**72**:1773-1783. DOI: 10.1158/0008-5472.CAN-11-3831

[48] Shi G, Monro S, Hennigar R, Colpitts J, Fong J, Kasimova K, et al. Ru(II) dyads derived from  $\alpha$ -oligothiophenes: A new class of potent and versatile photosensitizers for PDT. *Coordination Chemistry Reviews*. 2015;**282**:127-138. DOI: 10.1016/j.ccr.2014.04.012

[49] Raaphorst GP, Heller DP, Bussey A, Ng CE. Thermal radiosensitization by 41°C hyperthermia during low dose-rate irradiation in human normal and tumour cell lines. *International Journal of Hyperthermia*. 1994;**10**:263-270. DOI: 10.3109/02656739409009347

[50] Fong J, Kasimova K, Arenas Y, Kaspler P, Lazic S, Mandel A, et al. A novel class of ruthenium-based photosensitizers effectively kills in vitro cancer cells and in vivo tumors. *Photochemical & Photobiological Sciences*. 2015;**14**:2014-2023. DOI: 10.1039/c4pp00438h

[51] Yu B, Ouyang C, Qiu K, Zhao J, Ji L, Chao H. Lipophilic tetranuclear ruthenium(II) complexes as two-photon luminescent tracking non-viral gene vectors. *Chemistry - A European Journal*. 2015;**21**:3691-3700. DOI: 10.1002/chem.201405151

[52] Lazic S, Kaspler P, Mandel A, Jewett MAS, Kulkarni G, Lilge L. MP61-06. Photodynamic therapy for non-muscle invasive bladder cancer mediated by instilled photosensitizer TLD-1433 and green light activation. *The Journal of Urology*. 2016;**195**:E805. DOI: 10.1016/j.juro.2016.02.880

[53] Thota S, Rodrigues DA, Crans DC, Barreiro EJ. Ru(II) compounds: Next-generation anticancer metallotherapeutics? *Journal of Medicinal Chemistry*. 2018;**61**:5805-5821. DOI: 10.1021/acs.jmedchem.7b01689

[54] Kulkarni GS, Lilge L, Mandel A, Perlis N, Nesbitt M, Dumoulin-White R, et al. TLD-1433 photodynamic therapy for BCG-unresponsive NMIBC - a phase IB clinical study. In: 19th Annual Meeting of the Society of Urologic Oncology (SUO). Phoenix, AZ, USA; 2018

[55] NIST: X-Ray Mass Attenuation Coefficients – Ruthenium. 2018. Available from <https://physics.nist.gov/PhysRefData/XrayMassCoef/ElemTab/z44.html> [Accessed: 26 December 2018]

[56] Mandel A, Kaspler P, Roufaiel M, Munegowda MA, Lilge L. X-ray and photon mediated in vitro and in vivo activity of ruthenium(II) compounds. In: 16th International Photodynamic Association (IPA) World Congress. Coimbra, Portugal; 2017

[57] Giering K, Lamprecht I, Minet O, Handke A. Determination of the specific heat capacity of healthy and tumorous human tissue. *Thermochimica Acta*. 1995;**251**:199-205. DOI: 10.1016/0040-6031(94)02047-R